

Timescales in heavy ion collisions *

MIKE LISA

Department of Physics, The Ohio State University

The study of high energy collisions between heavy nuclei is a field unto itself, distinct from nuclear and particle physics. A defining aspect of heavy ion physics is the importance of a bulk, self-interacting system with a rich space-time substructure. I focus on the issue of timescales in heavy ion collisions, starting with proof from low-energy collisions that femtoscopy can, indeed, measure very long timescales. I then discuss the relativistic case, where detailed measurements over three orders of magnitude in energy reveal a timescale increase that might be due to a first-order phase transition. I discuss also consistency in evolution timescales as determined from traditional longitudinal sizes and a novel analysis using shape information.

The slowly crawling ants will eat our dreams.

- *Andrzej Białas, musing on words of Andre Breton*

Go to the ant, thou sluggard; consider her ways, and be wise.

- *Proverbs vi.6*

1. Preface

In the quote above, made at the first Workshop on Particle Correlations and Femtoscopy in the Czech Republic, Professor Białas was expressing a frustration felt periodically by those of us who labor to understand deeply the fascinating features of soft-scale QCD as manifest in the quark-gluon plasma, a bulk thermodynamic system of deconfined colored partons as degrees of freedom. Every time we gain a deeper insight into the physics and phenomenology of this system (the dream), more detailed theories (the ants) or experimental observations make clear that the system is more complicated than we thought. New advances often raise more questions than they answer.

Professor Białas made this statement with a smile on his face, however. He clearly considers himself an ant in the spirit of the quote from Proverbs:

* Written for the symposium in honor of Andrzej Białas 80th birthday

a worker with a mission much larger than himself, destined to build, piece by piece over the course of his life, an edifice in pursuit of that mission. He clearly relishes this role.

It turns out that this symposium is held shortly before a milestone birthday of my own, and I found myself contemplating my own much less impressive anthills. One topic I have returned to repeatedly in various forms is the timescale of the system formed in a heavy ion collision. Here, I discuss previous studies (and one unpublished analysis) to show the development of our understanding of these timescales as measured with two-particle intensity interferometry.

2. Introduction

To the general public, the field of heavy ion physics resembles high energy particle physics. The accelerators, the collaborations, and the detectors are mammoth. Papers are written by committee, and talks are selected according to the bylaws set by Councils and led by elected management teams. Students are well-versed in the particle zoo (often much more so, than their professors who grew up as nuclear physicists).

The origins of the field, however, lie more in the realm of nuclear physics. Concepts were developed and people trained in heavy ion experiments at facilities like GANIL, SIS/GSI, and the NSCL/MSU cyclotron facility. Pions were rare and almost exotic. Students were relatively well-versed in nuclear physics.

However, heavy ion physics is a field of its own—neither nuclear physics (which strives to understand the nucleus in its seemingly infinite complexity) nor particle physics (which attempts to bypass the complexity of all interactions to study symmetries manifest as particles). In heavy ion physics, we seek to create and study a new *system*. Ideally, it will be a nearly thermalized system, so that we may study its equation of state. At lower energies, the equation of state of highly compressed, cold matter provides information relevant to the cores of neutron stars [1]. In ultrarelativistic energies, the equation of state of colored matter near the deconfinement transition probes QCD under the most extreme conditions [2].

The hot system is self-interacting and characterized by detailed flow fields. Its femtoscopic substructure is dynamic and rich, with long lifetimes, anisotropic shapes, correlations between momentum and space-time, and whirling vortices. To understand the evolution of this substructure, it is important to obtain measures of the timescales involved. Figure 1 identifies two of them, for the case of ultrarelativistic collisions. Unfortunately, they are often conflated, using the ambiguous term “lifetime;” however, they are different, and it is best to keep the distinction clear. The evolution

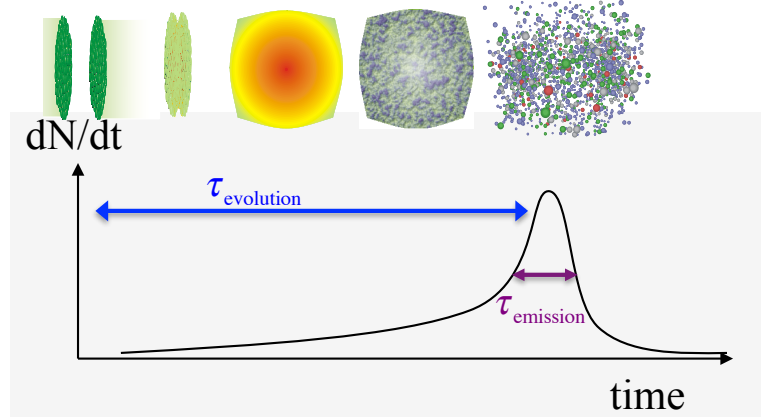


Fig. 1. The evolution of an ultra-relativistic heavy ion collision is sketched to indicate two relevant timescales, corresponding to the evolution of the entire system and the duration of the freezeout process. See text for details.

timescale $\tau_{\text{evolution}}$ refers to the time between initial interpenetration and particle freezeout. (Particles “freeze out” when they cease interacting with each other and the system.) Meanwhile, τ_{emission} refers to the duration of the freezeout process itself.

3. Can femtoscopy measure long emission durations?

The technique of two-particle intensity interferometry is a well-developed tool to extract spatio-temporal information from dynamic subatomic sources. Also known as femtoscopy, it exploits the fact that, given the observation of one particle, the conditional probability to measure a second particle depends on the relative momentum (measured) and the relative space-time position (inferred, by measuring the conditional probability) of the pair. For details and compilations of results, I refer the reader to reviews at both low [3] and high [4] energy collisions.

In principle, information about both space and time scales may be extracted by studying multi-dimensional correlation functions in the “out-side-long” (or, for low energies, the “longitudinal-transverse”) system of Bertsch and Pratt [5, 6]. Here, the “out” (or, for low energies, the “longitudinal”) direction is parallel to the direction of motion of the particles, while the “side” (or “transverse”) is perpendicular to it. A long emission duration (τ_{emission}) will generate a particle distribution extended in the direction of particle motion, and the resulting correlation will be less if the relative momentum is oriented in this direction. Emission duration measurements are of particular interest, because a first-order phase transition from a decon-

fined to a confined state, is expected to extend the emission time [5, 6, 7].

Through the early nineties, no emission duration greater than ~ 2 fm/c had been observed in the correlation data; indeed, most extracted timescales were consistent with zero. For the newly available collisions at the multi-GeV scale [4], this was a disappointing development, though perhaps not shocking. However, at non-relativistic energies available at NSCL and GANIL, this was surprising indeed. At these lower energies, the collision and evolution dynamics were believed to be better understood. Repeated reports of vanishing timescales from correlation measurements led some experts at the time to wonder whether the femtoscopic technique itself was sufficiently well understood ¹.

Could femtoscopy really measure timescales, after all? Two publications [9, 12] on proton correlations answered this important question with a resounding affirmative. In one, near multifragmentation energies, a lifetime greater than 10 fm/c was finally extracted from femtoscopic data. In the other, at compound nucleus energies, a lifetime greater than 1000 fm/c (!!) was reported. Both timescales were of the order of theoretical expectations.

Why had all previous published results reported no difference between longitudinal and transverse correlation functions, and hence emission timescales consistent with zero? The reason turned out to be simple: at least in the U.S., we had all been looking in the wrong frame.

3.1. A study of collisions at “intermediate” energies

Two-proton correlation functions at small relative momenta probe the space-time geometry of the emitting system, because the magnitude of nuclear and Coulomb final-state interaction and antisymmetrization effects depends on the spatial separation of the emitted particles [10]. The attractive S-wave nuclear interaction leads to a pronounced maximum in the correlation function at relative momentum $q = 20$ MeV/c. This maximum decreases for increasing source dimensions and/or emission time scales. The Coulomb interaction and antisymmetrization produce a minimum at $q = 0$. Nonspherical phase-space distributions, predicted for long-lived emission sources, can lead to a dependence of the two-proton correlation function on the direction of the relative momentum [8]. Until 1993, however, such directional dependences had not yet been observed unambiguously. The first observation was published in 1993 [9].

The experiment was performed at the National Superconducting Cyclotron Laboratory at Michigan State University (MSU). A beam of Ar ions at $E/A=80$ MeV incident energy and intensity $\sim 3 \times 10^8$ /sec bombarded a Sc target of areal density 10 mg/cm. Charged particles were measured

¹ Scott Pratt, 1992, private communication

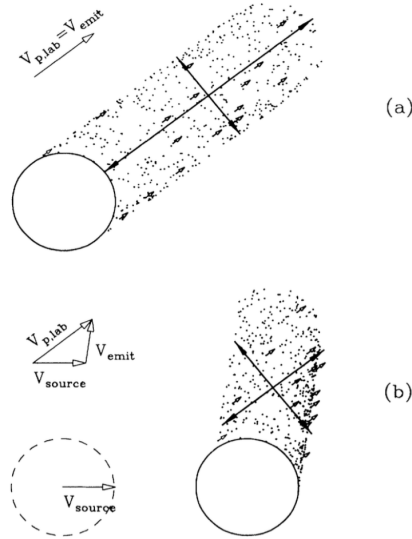


Fig. 2. Schematic illustration of phase-space distributions at a time $t = 70$ fm/c, seen by a detector at $\theta_{\text{lab}} = 38^\circ$, for a spherical source of radius $r = 3.5$ fm and lifetime $\tau = 70$ fm/c emitting protons of momentum 250 MeV/c. (a) Source at rest in the laboratory. (b) Source moves with $v_{\text{source}} = 0.18c$. In the phase-space distributions, the laboratory velocities of the emitted particles ($\vec{v}_{\text{p,lab}}$) are depicted by small arrows, and the directions perpendicular and parallel to $\vec{v}_{\text{p,lab}}$ are depicted by the large double-headed arrows. In (a) and (b), $\vec{v}_{\text{p,lab}}$ is kept constant, and \vec{v}_{emit} is different; therefore, the elongations along \vec{v}_{emit} are different. From [9].

in the MSU 4π Array, which consisted of 209 plastic $\Delta E - E$ phoswich detectors covering polar angles between $7^\circ - 158^\circ$ in the laboratory frame. One of the hexagonal modules of the 4π Array, located at 38° in the laboratory frame, was replaced by a 56-element high-resolution hodoscope. Each $\Delta E - E$ telescope of the hodoscope consisted of a $300 - \mu\text{m}$ -thick Si detectors backed by a 10-cm-long CsI(Tl) detector and subtended a solid angle of $\Delta\Omega = 0.37$ msr. The energy resolution was about 1% for 60 MeV protons; this is important for measuring large source sizes.

The problem of identifying finite emission duration is illustrated in Figure 2. It depicts phase-space distributions in the laboratory rest frame of protons emitted with fixed laboratory velocity $\vec{v}_{\text{p,lab}}$ towards the detector at $\theta_{\text{lab}} = 38^\circ$ for a source at rest in the laboratory (a) and for a source at rest in the center-of-momentum system of the projectile and target ($v_{\text{source}} = 0.18c$). We assumed a spherical source of 7 fm diameter and 70 fm/c lifetime emitting protons of momentum 250 MeV/c.

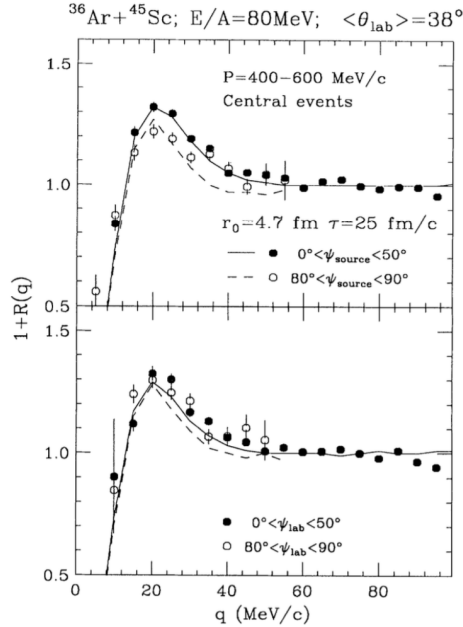


Fig. 3. Measured longitudinal and transverse correlation functions for protons emitted in central $^{36}\text{Ar} + ^{45}\text{Sc}$ collisions at $E/A = 80$ MeV. The correlation functions are shown for proton pairs of total laboratory momentum $P = 400 - 600$ MeV/c detected at $\langle\theta_{\text{lab}}\rangle = 38^\circ$. Longitudinal and transverse correlation functions (solid and open points, respectively) correspond to $\psi = \cos^{-1}(\vec{q} \cdot \vec{P}/qP) = 0^\circ - 50^\circ$ and $80^\circ - 90^\circ$, respectively. Solid and dashed curves represent longitudinal and transverse correlation functions predicted for emission from a spherical Gaussian source with $r_0 = 4.7$ fm and $\tau = 25$ fm/c, moving with $v_{\text{source}} = 0.18c$. Upper panel: \vec{P} and ψ are defined in the rest frame of the presumed source. Lower panel: \vec{P} and ψ are defined in the laboratory frame. From [9].

For emission from a source at rest, the phase-space distribution of particles moving with fixed velocity $\vec{v}_{\text{p,lab}} = \vec{v}_{\text{emit}}$ towards the detector exhibits an elongated shape oriented parallel to $\vec{v}_{\text{p,lab}}$. A source of lifetime τ_{emission} appears elongated in the direction of the proton momentum by an incremental distance $\Delta\vec{s} \approx \vec{v}_{\text{emit}} \cdot \tau_{\text{emission}} = \vec{p}_{\text{p,lab}}$. Correlation functions for relative momenta $\vec{q} \perp \vec{v}_{\text{p,lab}}$ reflect a stronger Pauli suppression, and hence a reduced maximum at $q \approx 20$ MeV/c, than those for $\vec{q} \parallel \vec{v}_{\text{p,lab}}$.

Cuts on the relative orientation of \vec{q} and \vec{P} are sensitive to the motion of the source, since the direction of the total momentum depends on the rest frame, while the direction of the relative momentum— at least in the

nonrelativistic limit— does not. (Note: the key to this result is not even a relativistic boost, but simply a Galilean one!) Previous analyses compared the shapes of the correlation functions selected by cuts on the relative angle $\psi_{\text{lab}} = \cos^{-1}(\vec{q} \cdot \vec{P}/qP)$ between \vec{q} and $\vec{P} = \vec{p}_1 + \vec{p}_2 \approx 2m\vec{v}_{\text{p,lab}}$, where \vec{p}_1 and \vec{p}_2 are the laboratory momenta of the two protons and \vec{q} is the momentum of relative motion. Such analyses are optimized to detect emission duration effects of sources stationary in the laboratory system, but they can fail to detect such effects for nonstationary sources. For the specific case illustrated in Fig. 2(b), the source dimensions parallel and perpendicular to $\vec{p}_{\text{p,lab}}$ are very similar, and no significant differences are expected for the corresponding longitudinal and transverse correlation functions.

For a source of known velocity, the predicted lifetime effect is detected most clearly if longitudinal and transverse correlation functions are selected by cuts on the angle $\psi_{\text{source}} = \cos^{-1}(\vec{q}' \cdot \vec{P}'/q'P')$, where the primed quantities are defined in the rest frame of the source. In the frame of the source, the phase-space distribution is always elongated in the direction of \vec{v}_{emit} . Hence, in Fig. 2(b), the source dimensions should be compared in directions parallel and perpendicular to \vec{v}_{emit} . Such analyses can only be carried out for emission from well-characterized sources.

Figure 3 corroborates this reasoning with experimental data. It shows longitudinal and transverse two-proton correlation functions for central Ar+Sc collisions at $E/A=80$ MeV selected by appropriate cuts on the total transverse energy detected in the 4π Array. In a geometrical picture, the applied cuts correspond to reduced impact parameters of $b/b_{\text{max}} = 0 - 0.36$. Longitudinal (solid points) and transverse (open points) correlation functions were defined by cuts on the angle $\psi = \cos^{-1}(\vec{q} \cdot \vec{P}/qP) = 0^\circ - 50^\circ$ and $80^\circ - 90^\circ$, respectively. The normalization constant C in Eq. (1) is independent of ψ . To maximize lifetime effects and reduce contributions from the very early stages of the reaction, the coincident proton pairs were selected by a low-momentum cut on the total laboratory momentum, $P = 400 - 600$ MeV/c. The top panel shows correlation functions for which the angle ψ was defined in the center-of-momentum frame of projectile and target ($\psi = \psi_{\text{source}}$); for central collisions of two nuclei of comparable mass, this rest frame should be close to the rest frame of the emitting source. The bottom panel shows correlation functions for which the angle ψ was defined in the laboratory frame.

Consistent with the qualitative arguments presented in Figure 2, a clear difference between longitudinal and transverse correlation functions is observed for cuts on ψ_{source} (top panel of figure 3) but not for cuts on ψ_{lab} (bottom panel of figure 3). The clear suppression of the transverse correla-

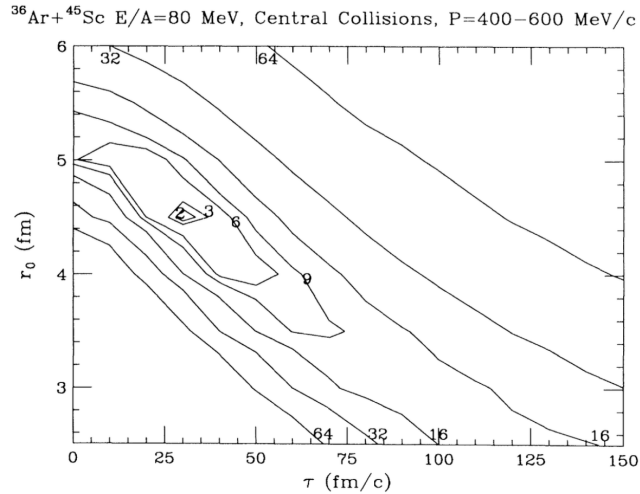


Fig. 4. Contour diagram of χ^2/ν determined by comparing theoretical correlation functions to the data shown in the upper panel of figure 3. The fit was performed in the peak region of the correlation function $q = 15 - 30$ MeV/c. From [9].

tion function with respect to the longitudinal correlation function observed in the top panel in Figure 3 is consistent with expectations for emission from a source of finite lifetime. The solid and dashed curves in the top and bottom panels of Figure 3 depict calculations for emission from a spherical Gaussian source comoving with the center-of-momentum frame of the projectile and target. The calculations were performed for the radius and lifetime parameters $r_0 = 4.7$ fm and $\tau_{\text{emission}} = 25$ fm/c. The calculations corroborate the qualitative arguments illustrated in Figure 2. The data in Figure 3 represent the first clear experimental evidence of this predicted lifetime effect.

For a more quantitative analysis, we performed calculations assuming a simple family of sources of lifetime and spherically symmetric Gaussian density profiles, moving with the center-of-momentum frame of reference. Energy and angular distributions of the emitted protons were selected by randomly sampling the experimental yield $Y(\vec{p})$. Specifically, the single particle emission functions were parametrized as

$$g(\vec{r}, \vec{p}, t) \propto \exp(-r^2/r_0^2 - t/\tau) Y(\vec{p}). \quad (1)$$

In equation 1, \vec{r} , \vec{p} , and t are understood as being in the rest frame of the source. Phase-space points generated in the rest frame of the source were Lorentz boosted into the laboratory frame, and the two-

proton correlation function was obtained by convolution with the two-proton relative wavefunction.

Transverse and longitudinal correlation functions were calculated for the range of parameters $r_0 = 2.5 - 6.0$ fm and $\tau = 0 - 150$ fm/c. For each set of parameters, the agreement between calculated and measured longitudinal and transverse correlation functions was evaluated by determining the value of χ^2/ν in the peak region, $q = 15 - 30$ MeV/c. A contour plot of χ^2/ν as a function of r_0 and τ is given in figure 4. Good agreement between calculations and data is obtained for source parameter values of roughly $r_0 \approx 4.5 - 4.8$ fm and $\tau \approx 20 - 40$ fm/c. These extracted emission time scales are qualitatively consistent with those predicted by microscopic transport calculations.

3.2. Very long emission durations from Xe+Al collisions

The measurement discussed in the previous section provided the first unambiguous observation of long emission durations with femtoscopy. It thus validated the technique— source lifetimes (emission durations) *can* be measured. For years, the problem had been that we were looking at longitudinal and transverse cuts in the wrong (laboratory) frame.

Dynamical models for symmetric systems with beam energies $E/A \approx 80$ MeV predict lifetimes ~ 20 fm/c, consistent with data, as we've seen. But *really* long lifetimes are predicted at lower excitation energies, where a compound nucleus is briefly formed and cools by nucleon emission.

A study of two-proton correlation functions in the inverse kinematics reaction Xe+Al at $E/A = 31$ MeV, reported [11] no difference between longitudinal and transverse correlation functions, although a very long lifetime ($\tau \sim 1000$ fm/c) would be expected. With the newfound insight on the importance of analyzing the data in the “right” (source) frame, we decided to extract the raw data from storage and perform a re-analysis.

The results are shown in figure 5. When we repeated the analysis of [11], we found no difference when cutting on ψ_{lab} , in agreement with the original published result. However, when we selected on the angle between \vec{q} and \vec{P} in the center-of-mass frame, a significant difference was observed [12]. The curves in figure 5 correspond to a spherical source, moving in the lab at $v_{\text{source}} = 0.2086c$ (the system center-of-momentum velocity), with radius and lifetime parameters $R = 3.5$ fm/c and $\tau = 1300$ fm/c, respectively.

Figure 6 quantifies the sensitivity of the parameter extraction, through contours of the chi-square per degree of freedom, analogous to that of figure 4.

This result is virtually unknown in the relativistic heavy ion community, which is unfortunate— 1300 fm/c! This value, which is precisely what one

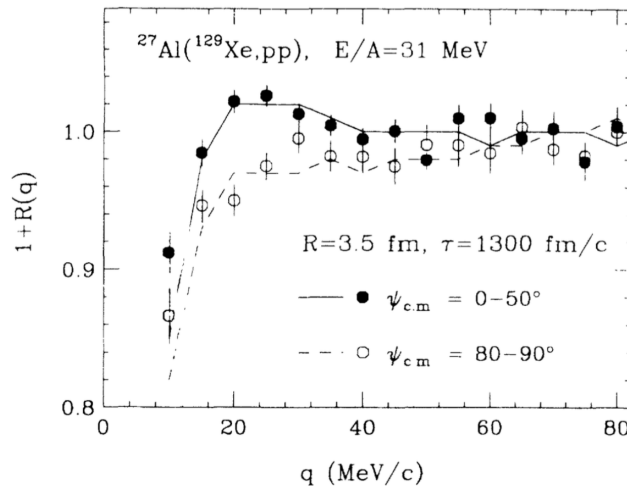


Fig. 5. Comparison of measured (points) and calculated (curves) correlation functions. The calculations were performed for emission from a schematic source with radius and lifetime parameters $R = 3.5$ fm and $\tau = 1300$ fm/c. From [12].

expects for an evaporating compound nucleus at this energy, remains the longest timescale ever measured with multidimensional intensity interferometry in subatomic physics.

4. Evidence for a burning log

There have long been predictions [5, 6, 7] that a first-order transition from a deconfined state (quark-gluon plasma) to a confined (hadronic) final state, may lead to an increase in the system emission time. The expectation [7] is that this increase should occur just at the threshold energy for which a deconfined state is formed. At lower energies there is no transition at all, whereas at higher energies the system is exploding too quickly to form a “burning log” scenario. The threshold energy samples the “softest point” in the QCD equation of state.

At the relativistic collision energies where this phenomenon might occur, studies have used multi-dimensional pion interferometry [4], where the relative momentum components (and corresponding “HBT radii”) are identified in the “Bertsch-Pratt” decomposition [5, 6]. Referring to figure 2, R_{out} measures the length scale of the pion cloud in the direction of the particle motion, and R_{side} quantifies the length scale perpendicular to this motion. (At relativistic energies, where the dynamics in the beam direction are substantially different from those in the transverse direction, R_{out} and R_{side} are

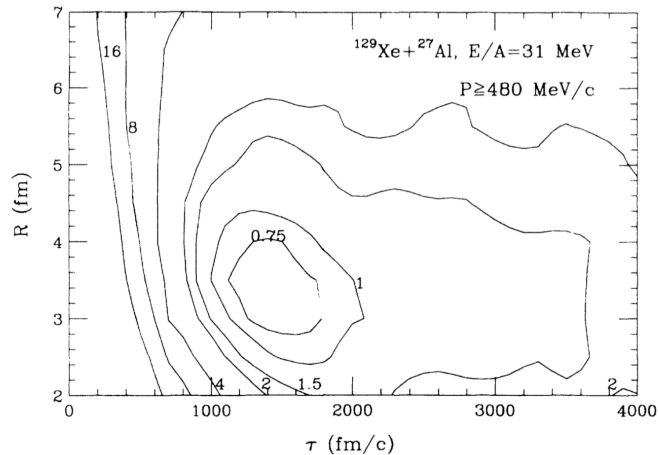


Fig. 6. Contour plot of χ^2/ν evaluated by comparing measured longitudinal and transverse correlation functions (over the range $15 \text{ fm}/c \leq q \leq 40 \text{ fm}/c$ to those predicted for emission from a schematic source with radius and lifetime parameters R and τ . From [12].

forced to be perpendicular to the beam direction, and a third radius, R_{long} quantifies the length scale along the beam. At the lower energies discussed in sections 3.1 and 3.2, where compound nucleus formation occurs, this distinction is not made in the “longitudinal-transverse” decomposition.) In the hypothetical case where the system is not flowing, these radii are related to the emission duration τ_{emission} as

$$R_{\text{out}}^2 \approx R_{\text{side}}^2 + \beta^2 \tau_{\text{emission}}^2, \quad (2)$$

where $\beta = p_{\perp}/E$ is the pion speed in the transverse direction. Relativistic heavy ion collisions, however, are dominated by transverse flow, so equation 2 is only a crude approximation [13]; indeed, R_{out} can be less than R_{side} at high p_T [14].

A review of femtoscopic results in 2005 [4] concluded that there was no evidence for the burning log signature in the two decades of relativistic heavy ion measurements at the AGS, SPS and RHIC. Since that review, another decade has passed, and many more measurements have been done. Figures 7 and 8 contain the world dataset of pion HBT radii from collisions of the heaviest nuclei (Au+Au in the U.S. and Pb+Pb in Europe).

Datapoints in the yellow panels correspond to measurements that were performed in last decade. ALICE measurements [15] at the LHC extend the measured energy range to three orders of magnitude. More important, however, are the measurements at RHIC and the SPS at energies *below*

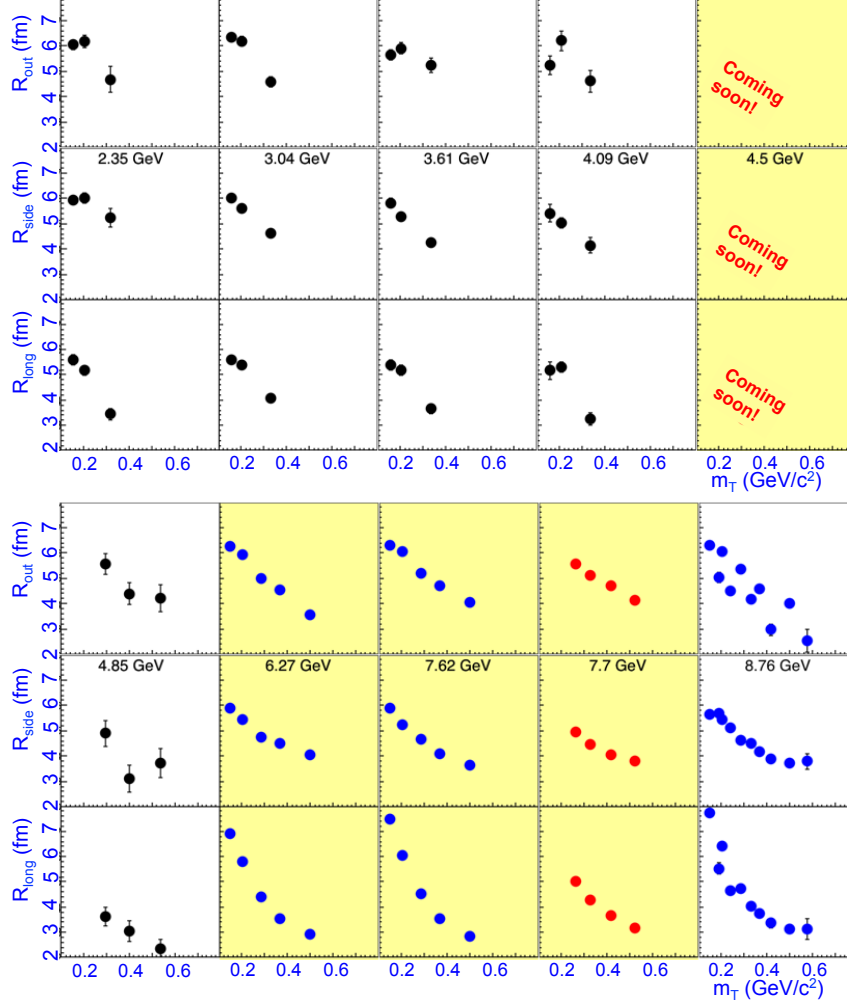


Fig. 7. Two-pion femtoscopy has been measured in central heavy ion collisions over three orders of magnitude. Above, HBT radii from $\sqrt{s_{NN}} = 2.35 - 8.76$ GeV collisions are plotted versus the transverse mass of the pair. Figure 8 shows analogous data up to $\sqrt{s_{NN}} = 2760$ GeV.

Black datapoints originate from experiments at the AGS; red datapoints originate from experiments at RHIC; blue datapoints originate from experiments at the SPS; pink datapoints originate from experiments at the LHC.

Yellow panels identify measurements done after a 2005 review [4].

the maximum energy of the machine. These data were taken in “energy scan” programs, motivated by the increasing realization that some of the

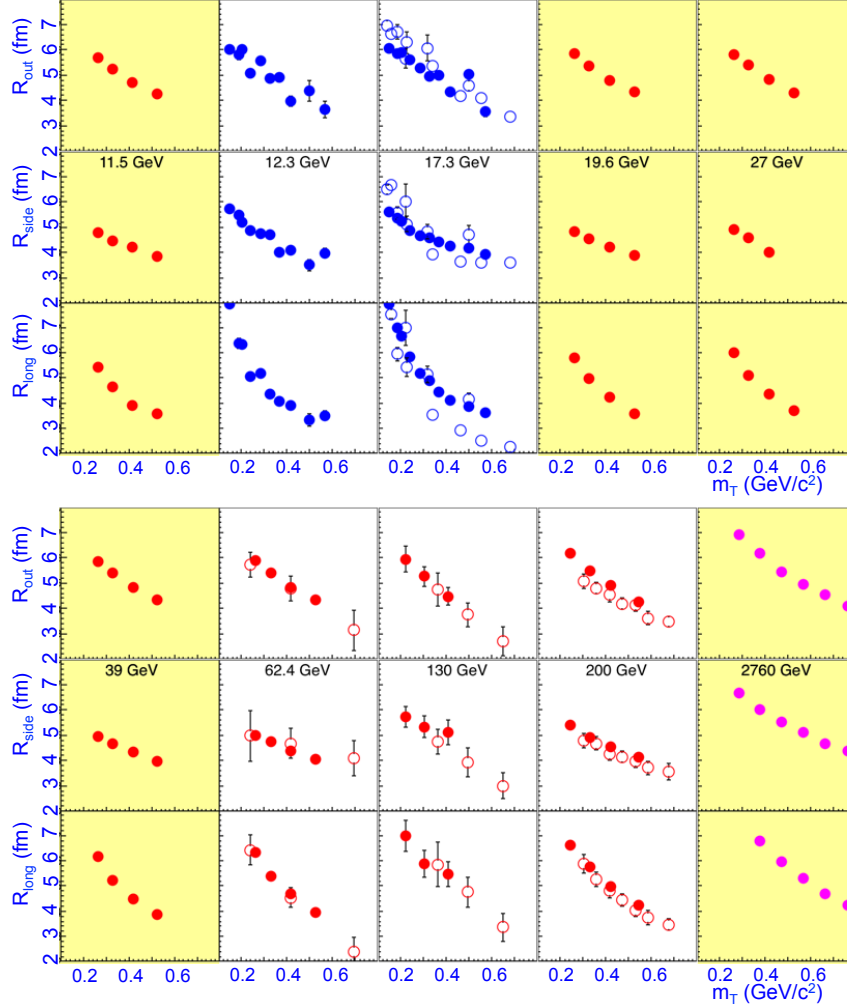


Fig. 8. Two-pion femtoscopy has been measured in central heavy ion collisions over three orders of magnitude. Above, HBT radii from $\sqrt{s_{NN}} = 11.5 - 2760$ GeV collisions are plotted versus the transverse mass of the pair. Figure 7 shows analogous data down to $\sqrt{s_{NN}} = 2.35$ GeV.

Black datapoints originate from experiments at the AGS; red datapoints originate from experiments at RHIC; blue datapoints originate from experiments at the SPS; pink datapoints originate from experiments at the LHC.

Yellow panels identify measurements done after a 2005 review [4].

most important phenomena in hot QCD physics might only be revealed by a careful, systematic study of heavy ion collisions as the system conditions

are gradually changed.

The versatility of the RHIC collider is clear from the fact that the RHIC data (red data points) extend to low energies well below traditional SPS energy of 17.3 GeV. STAR has collected data in “fixed-target mode,” in which one low-energy RHIC beam struck a gold foil placed toward the edge of the beam pipe at one end of the STAR detector. Despite the fact that STAR is designed for midrapidity measurements at a 200-GeV collider, the data taken were good, and HBT radii, fully in line with data at similar energies, have been measured. At this moment, these results are unavailable for release; however, they are firm, and I could not resist a placeholder in figure 7 indicating that RHIC has now extended measurements into the AGS energy range.

The energy scan at RHIC may have finally revealed the burning log signature, as shown in figure 9. A clear peak in $R_{\text{out}}^2 - R_{\text{side}}^2$ (or $R_{\text{out}}/R_{\text{side}}$ [14]) is observed around $\sqrt{s_{NN}} = 15$ GeV, an energy region where other intriguing phenomena have been reported [16, 17]. This figure includes only data from RHIC and LHC collider experiments; these have all been performed with similar techniques and acceptances. Experiments at the CERN SPS have acceptances which vary with $\sqrt{s_{NN}}$, making them not ideal for searching for subtle changes as collision energy changes; femtoscopic results fluctuate significantly and disagree experiment-to-experiment. Furthermore, SPS measurements are performed with a variety of methods to handle the Coulomb effect; this can affect HBT radii significantly [18]. RHIC and LHC experiments all use the so-called Bowler-Sinyukov [19, 20] approach, explicitly including Coulomb effects in the fits to the correlation functions.

It is increasingly important that hydrodynamic theory address the RHIC Beam Energy Scan range in detail. While calculations at LHC energies are technically easier to perform (due to approximate boost invariance, a simple Equation of State, and low viscosity), the lower energies are more important. QCD has a scale, after all. Just as solid state physicists study superconductivity around the transition point, heavy ion studies must focus on the energy region set by QCD physics.

5. The evolution time of the system

Thus far, I have discussed measurements of the emission duration τ_{emission} of the hot system generated in a heavy ion collision. An estimate of the evolution timescale, $\tau_{\text{evolution}}$, is also crucial for a detailed understanding of the system’s dynamics.

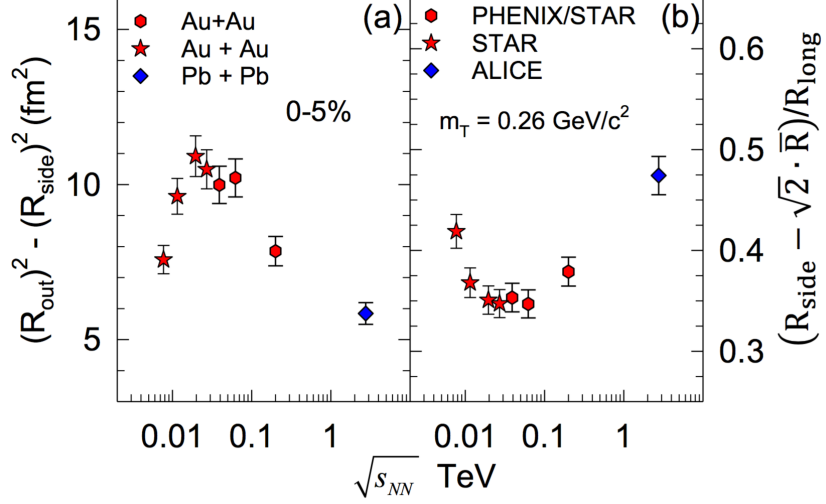


Fig. 9. The difference (or ratio) of R_{out} and R_{side} is related to the emission duration of the collision. As discussed in the text, a generic expectation from a first-order phase transition is a rise and fall of this difference, with collision energy. Data from the RHIC Beam Energy Scan appears to validate this prediction. Figure from [21].

5.1. Estimate based on the longitudinal radius

At the very low energies discussed in sections 3.1 and 3.2, it is unclear how to distinguish the system evolution time from the emission duration. However, as Sinyukov and collaborators pointed out [22], in ultrarelativistic collisions, the strong longitudinal flow generates a nearly boost-invariant system in which the longitudinal HBT radius and evolution time are related by [22, 23]

$$R_{\text{long}}^2(m_T) \approx \tau_{\text{evolution}}^2 \frac{T}{m_T} \frac{K_2(m_T/T)}{K_1(m_T/T)}, \quad (3)$$

where T is the system temperature at freezeout, and m_T is the transverse mass of the particles.

Figure 10 shows fits of formula 3 to longitudinal radii measured [18] by the STAR Collaboration for collisions at $\sqrt{s_{NN}} = 200$ GeV at various centralities. The fit is reasonable. Evolution timescales extracted from STAR [14] and ALICE [15] are shown in figure 11.

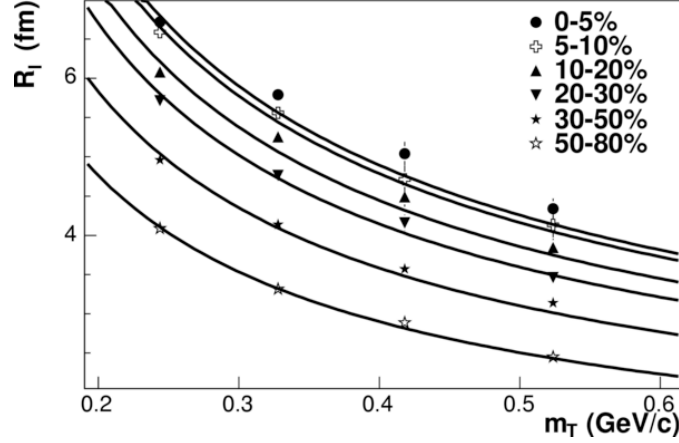


Fig. 10. Longitudinal HBT radii for $\sqrt{s_{NN}} = 200$ GeV Au+Au collisions of varying centrality, measured by the STAR Collaboration. From [18].

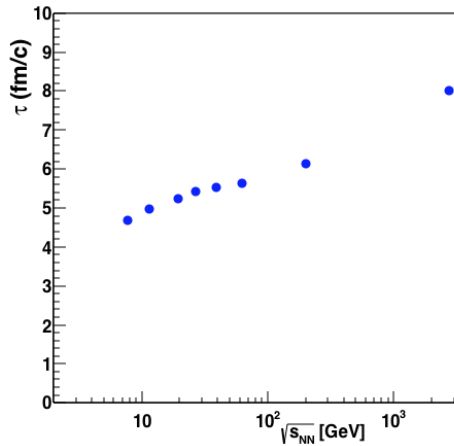


Fig. 11. Estimate of the system evolution time based on Sinyukov fits (equation 3) to measured longitudinal HBT radii R_{long} .

5.2. Alternate cross-check of the evolution time estimate

In section 5.1, I outlined the “traditional” way to estimate the evolution time, based on the m_T dependence of the longitudinal HBT radius. Here, I provide an independent cross-check from another direction.

In non-central heavy ion collisions, the hot system is initially anisotropic relative to the reaction plane (spanned by the impact parameter vector and the beam direction) of the collision. The response of the system to this coordinate-space anisotropy generates a corresponding momentum-space

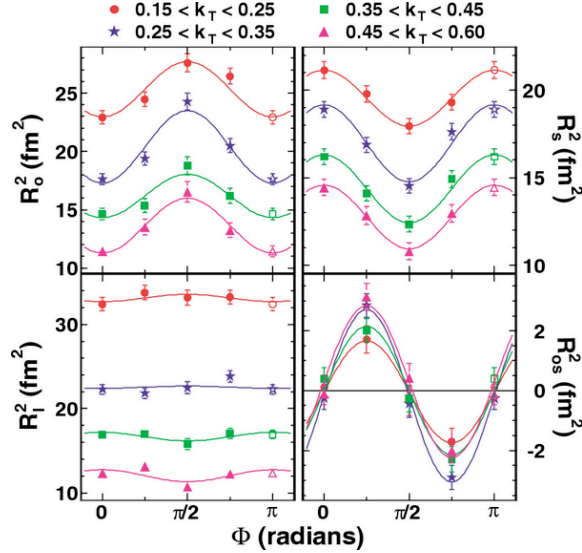


Fig. 12. Pion HBT radii from mid-central Au+Au collisions at $\sqrt{s_{NN}} = 200$ GeV, as a function of azimuthal angle relative to the event plane. From [27].

anisotropy, in which more (and faster) particles are emitted in the reaction plane than perpendicular to it. This is the well-known “elliptic flow” phenomenon, often quantified by a momentum-space anisotropy parameter v_2 [24].

The preferentially in-plane expansion will tend to reduce (or perhaps reverse) the anisotropy of the initial state; i.e. the system will become more round in coordinate space. If the system retains some anisotropy, the transverse HBT radii will oscillate as a function of azimuthal angle relative to the reaction plane [25, 26, 13]. Figure 12 shows femtoscopic radii measured [27] by the STAR Collaboration for mid-central Au+Au collisions at $\sqrt{s_{NN}} = 200$ GeV. Fourier coefficients, the space-time analog to v_2 , may be extracted from the oscillations and used to estimate the spatial anisotropy of the source at freeze-out [13], defined as

$$\epsilon_F \equiv \frac{\sigma_y^2 - \sigma_x^2}{\sigma_y^2 + \sigma_x^2}, \quad (4)$$

where σ_x (σ_y) is the root-mean-square extent of the source in (out of) the event plane.

Spatial anisotropies have been extracted for heavy ion collisions over the entire available energy range and are plotted in figure 13. For all energies, the system retains its out-of-plane extension in coordinate space, though it is reduced from its initial value of 0.25 (estimated from Glauber calculations).

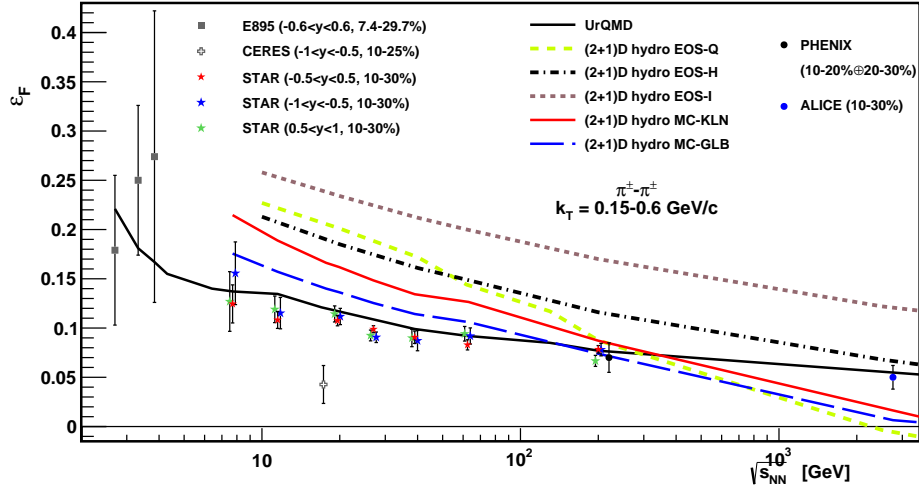


Fig. 13. The spatial anisotropy, defined in equation 4, for mid-central Au+Au (Pb+Pb) collisions from E895/AGS [25], CERES/SPS [28], STAR/RHIC [27, 14], PHENIX/RHIC [29] and ALICE/LHC [30]. Calculations [31, 32, 33] with hydrodynamic and transport models are shown for comparison.

The evolution of the hot system produced in a heavy ion collision is complex, but toy models can be useful to check whether disparate measurements may be understood in a single simple scenario. In this spirit, I construct a blast-wave [13] inspired model and ask whether the evolution times plotted in figure 11 are reasonably consistent with the reduction in coordinate-space anisotropy seen in figure 13.

Let $\bar{\sigma}_0$ be the angle-averaged RMS size of the source at $t = 0$, and ϵ_0 be its anisotropy. Further, let β_x and β_y be the average flow velocities in and out of the reaction plane. Assuming constant anisotropic free-streaming evolution of the source, its spatial anisotropy after evolving for $\tau_{\text{evolution}}$ is

$$\epsilon_F(\tau_{\text{evolution}}) = \frac{\bar{\sigma}_0^2 \epsilon_0 - \frac{1}{2} (\beta_y^2 - \beta_x^2) \tau_{\text{evolution}}^2}{\bar{\sigma}_0^2 \epsilon_0 + \frac{1}{2} (\beta_y^2 + \beta_x^2) \tau_{\text{evolution}}^2} \quad (5)$$

Based on Glauber calculations, $\sigma_0 \approx 3.5$ fm and $\epsilon_0 \approx 0.25$. The evolution time $\tau_{\text{evolution}}$ for the 10-30% central collisions were extracted from R_{long} for that centrality. Average transverse flow velocities are related to blast-wave [13] flow parameters according to

$$\beta_y = \tanh(2(\rho_0 - \rho_2)/3) \quad \beta_x = \tanh(2(\rho_0 + \rho_2)/3).$$

Using blast-wave fit parameters extracted by the PHENIX collaboration [34], $\beta_x = 0.585$ and $\beta_y = 0.490$. While one expects higher flow velocities at

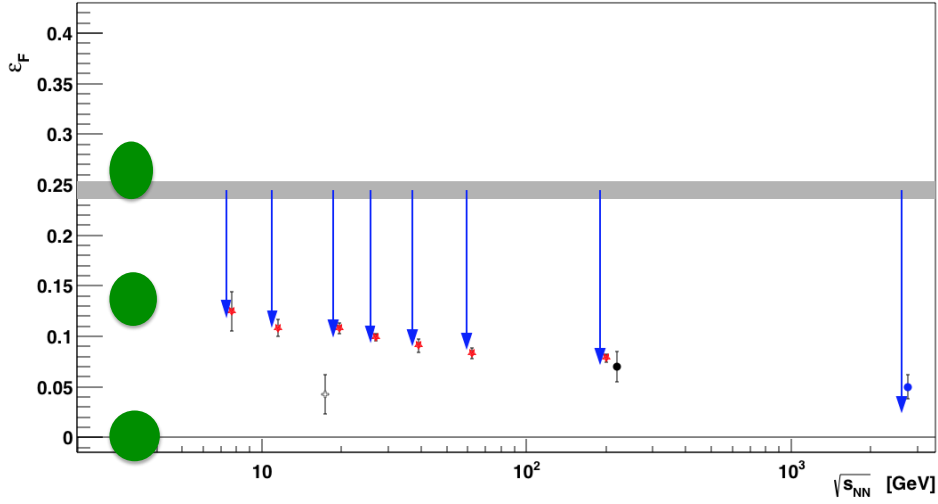


Fig. 14. Measurements of the final freeze-out eccentricity (from figure 13) are compared with calculations of a toy model based on an initially out-of-plane extended source evolving with preferential in-plane expansion. The grey band indicates the initial anisotropy based on Glauber calculations, and the downward-facing arrows indicate the evolution of the shape. The terminus of the arrow corresponds to the shape size at the time $\tau_{\text{evolution}}$ extracted by Sinyukov fits (equation 3 to the longitudinal radii. See equation 5 and text for details.

higher energies, the same values for β_x and β_y were used for all $\sqrt{s_{NN}}$, since other blast-wave fits were not readily unavailable. However, it turns out that these velocities vary little with $\sqrt{s_{NN}}$, so these values should serve for a test.

The estimate from this toy model is compared to data in figure 14. Considering its crudity and not tinkering with parameters, the agreement is remarkable. Both the magnitude and the $\sqrt{s_{NN}}$ -dependence of ϵ_F seem to be consistent with an evolution timescale extracted in the “traditional” way, using R_{long} , as discussed in section 5.1.

6. Summary

To understand the dynamics of a heavy ion collision, it is important to have an estimate of the timescales associated with its evolution. I have discussed experimental measurements of the emission and evolution timescales based on particle intensity interferometry measurements.

When the analysis was performed in the correct reference frame, two-proton correlation functions at low collision energies revealed long lifetimes,

consistent with theoretical expectations. These observations were important, as they put to rest troubling doubts about our understanding of intensity interferometry overall.

In ultra-relativistic heavy ion collisions, the long-sought “burning log” signature of a softening of the equation of state was found, but only after a systematic scan of the collision energy. This is one of several interesting signatures at energies around $\sqrt{s_{NN}} \approx 20$ GeV that have been revealed in the RHIC Beam Energy Scan program.

The evolution time of a collision is found to grow with collision energy, and the traditional estimate based on the longitudinal HBT radius was found to be consistent with a toy model describing the evolution of the spatially anisotropic source as estimated by azimuthal oscillations of the transverse HBT radii.

These timescale estimates serve as important input to theoretical studies of the dynamics of the collision. Such studies are crucial, if the field is to generate lasting physics contributions to our understanding of QCD. While dynamic modeling of the highest-energy collisions (e.g. at the LHC) are much easier, it is much more important to focus on lower energies around $\sqrt{s_{NN}} \sim 20$ GeV, where nontrivial phenomena associated with the QCD equation of state may appear.

Finally, I would like to congratulate Prof. Andrzej Białas on the occasion of his 80th birthday, from one ant to another.

REFERENCES

- [1] M. B. Tsang, et al., *Prog. Part. Nucl. Phys.* **66**, 400 (2011).
- [2] Edward Shuryak, *Prog. Part. Nucl. Phys.* **62**, 48 (2009).
- [3] D. H. Boal, C. K. Gelbke, B. K. Jennings, *Rev. Mod. Phys.* **62**, 553 (1990).
- [4] Michael Annan Lisa, Scott Pratt, Ron Soltz, Urs Wiedemann, *Ann. Rev. Nucl. Part. Sci.* **55**, 357 (2005).
- [5] S. Pratt, *Phys. Rev.* **D33**, 1314 (1986).
- [6] G. F. Bertsch, *Nucl. Phys.* **A498**, 173C (1989).
- [7] Dirk H. Rischke, Miklos Gyulassy, *Nucl. Phys.* **A608**, 479 (1996).
- [8] S. Pratt, M. B. Tsang, *Phys. Rev.* **C36**, 2390 (1987).
- [9] M. A. Lisa, et al., *Phys. Rev. Lett.* **71**, 2863 (1993).
- [10] S. E. Koonin, *Phys. Lett.* **B70**, 43 (1977).
- [11] W. G. Gong, et al., *Phys. Rev.* **C43**, 1804 (1991).
- [12] M. A. Lisa, et al., *Phys. Rev.* **C49**, 2788 (1994).
- [13] Fabrice Retiere, Michael Annan Lisa, *Phys. Rev.* **C70**, 044907 (2004).
- [14] L. Adamczyk, et al., *Phys. Rev.* **C92**, 014904 (2015).

- [15] Jaroslav Adam, et al., *Phys. Rev.* **C93**, 024905 (2016).
- [16] L. Adamczyk, et al., *Phys. Rev. Lett.* **112**, 032302 (2014).
- [17] L. Adamczyk, et al., *Phys. Rev. Lett.* **112**, 162301 (2014).
- [18] J. Adams, et al., *Phys. Rev.* **C71**, 044906 (2005).
- [19] M. G. Bowler, *Phys. Lett.* **B270**, 69 (1991).
- [20] M. G. Bowler, *Z. Phys.* **C39**, 81 (1988).
- [21] A. Adare, et al., arxiv:1410.2559 (2014).
- [22] A. N. Makhlin, Yu. M. Sinyukov, *Z. Phys.* **C39**, 69 (1988).
- [23] U. A. Wiedemann, et al., *Phys. Rev.* **C52**, 918 (1996).
- [24] Sergei A. Voloshin, Arthur M. Poskanzer, Raimond Snellings (2008). arxiv:0809.2949 (2008).
- [25] Michael Annan Lisa, Ulrich W. Heinz, Urs Achim Wiedemann, *Phys. Lett.* **B489**, 287 (2000).
- [26] Ulrich W. Heinz, A. Hummel, M. A. Lisa, U. A. Wiedemann, *Phys. Rev.* **C66**, 044903 (2002).
- [27] J. Adams, et al., *Phys. Rev. Lett.* **93**, 012301 (2004).
- [28] D. Adamova, et al., *Phys. Rev.* **C78**, 064901 (2008).
- [29] A. Adare, et al., *Phys. Rev. Lett.* **112**, 222301 (2014).
- [30] Vera Loggins, *Nucl. Phys.* **A931**, 1088 (2014).
- [31] Peter F. Kolb, Ulrich W. Heinz (2003). arxiv nucl-th/0305084 (2003).
- [32] M. A. Lisa, E. Frodermann, G. Graef, M. Mitrovski, E. Mount, H. Petersen, M. Bleicher, *New J. Phys.* **13**, 065006 (2011).
- [33] Chun Shen, Ulrich Heinz, *Phys. Rev.* **C85**, 054902 (2012), [*Erratum: Phys. Rev.C86,049903(2012)*].
- [34] A. Adare, et al., *Phys. Rev.* **C92**, 034914 (2015).